


## Enhanced diamagnetism by energetic tail electrons in a magnetized plasma

Kazunori Takahashi <sup>1,2,\*</sup>, Christine Charles <sup>3</sup> and Rod W. Boswell<sup>3</sup>

<sup>1</sup>*Department of Electrical Engineering, Tohoku University, Sendai 980-8579, Japan*

<sup>2</sup>*Interdisciplinary Research Center for Non-equilibrium Plasma, Tohoku University, Sendai 980-8579, Japan*

<sup>3</sup>*Space Plasma, Power and Propulsion Laboratory, Research School of Physics, The Australian National University, Canberra ACT 2601, Australia*



(Received 14 December 2022; accepted 27 March 2023; published 11 May 2023)

Measurement of an internal azimuthal plasma current in a collisionless low  $\beta$  plasma expanding in a magnetic nozzle is presented. The electric field is removed from the plasma ensuring a negligible electron  $\mathbf{E} \times \mathbf{B}$  drift resulting in a purely diamagnetic electron azimuthal current. The electron energy probability function is non-Maxwellian, having an energetic tail component in addition to the thermal bulk electrons. The measured azimuthal current is significantly larger than the electron diamagnetic current estimated by considering only the bulk electrons. This can be well explained by considering the energetic tail electrons, which have a density of only about five percent of the total density. These results experimentally demonstrate that the energetic tail electrons are major contributors to the diamagnetism of the plasma even if their density is a small fraction of the total electron density.

DOI: [10.1103/PhysRevResearch.5.L022029](https://doi.org/10.1103/PhysRevResearch.5.L022029)

Diamagnetism is a fundamental and inherent characteristic of magnetized plasmas and distorts the external magnetic fields by reducing the field strength inside the plasma [1]. This can be often characterized by  $\beta$  given by the ratio of the plasma pressure to the external magnetic field pressure. Due to significant changes in the magnetic fields for high  $\beta$  plasmas, various phenomena can be observed in natural and terrestrial plasmas, e.g., modification of the earth's magnetic field [2], auroral substorms [3], magnetic holes in the solar wind and near a comet [4], and field-reversed configuration for fusion reactor [5]. Even for low  $\beta$  plasmas, analytical, numerical, and experimental studies have shown that the diamagnetism significantly contributes to the momentum conversion process in an expanding magnetic field commonly called a magnetic nozzle [6–8].

The diamagnetism is often governed by a pressure balance of  $\nabla(p + B^2/2\mu_0) = 0$  in a magnetohydrodynamic (MHD) approximation, where  $p$ ,  $B$ , and  $\mu_0$  are the plasma pressure, the magnetic field including both the external and plasma-induced components, and the magnetic permeability in vacuum, respectively. This implies that it is possible to reduce the magnetic field pressure in the plasma compared with the vacuum magnetic field. The diamagnetic behavior originates from internal plasma currents generating a magnetic field opposite to the externally applied magnetic field. However, the reduction of the magnetic field strength in

low-temperature laboratory plasmas has often been smaller than that expected from the MHD pressure balance, even for high  $\beta$  conditions. Under these weakly magnetized conditions the effects of electric fields [9], magnetic field penetration and dissipation [10], and the neutral pressure [11] have been discussed.

In weakly magnetized, low  $\beta$ , and collisionless laboratory plasmas, the plasma potential is generally finite and electric fields perpendicular to the magnetic fields spontaneously develop, which affect the force balance of the electrons [9]. For the case where the ion temperature/pressure are negligible and a finite ion Larmor effect reduces the ion  $\mathbf{E} \times \mathbf{B}$  drift current, the momentum equation of the electrons can provide the azimuthal electron current  $j_{\theta e}$  due to both the electron diamagnetic and  $\mathbf{E} \times \mathbf{B}$  drift currents [12]. Therefore, the diamagnetism of the plasma is modified by the electric field. Furthermore, the electron energy distributions are assumed to be Maxwellian for both the MHD and fluid approximations, while electron energy probability functions (EEPFs) frequently deviate from Maxwellian distributions in a variety of plasmas, e.g., as observed in the Van Allen belts [13], solar wind [14], laser plasmas [15], magnetically-confined fusion plasma reactors [16], and low-pressure cathodic and radiofrequency plasmas [17–20]. Investigating the diamagnetism resulting from non-Maxwellian electrons is essential to understand the interaction of the plasma with external magnetic fields. However, the effect of non-Maxwellian electrons on the diamagnetism is difficult to quantitatively investigate in laboratory experiments due to the superposition of the electric field effect, i.e., the  $\mathbf{E} \times \mathbf{B}$  drift current, despite the important and fundamental problem relating to the various plasma phenomena in the majority of observations, experiments, and models.

Here the diamagnetic effect for the particular non-Maxwellian EEPFs containing tail electrons is experimentally

\*kazunori.takahashi.e8@tohoku.ac.jp

Published by the American Physical Society under the terms of the [Creative Commons Attribution 4.0 International](https://creativecommons.org/licenses/by/4.0/) license. Further distribution of this work must maintain attribution to the author(s) and the published article's title, journal citation, and DOI.

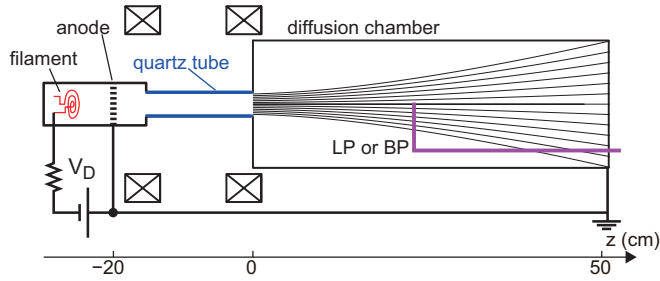


FIG. 1. Schematic of the experimental setup.

investigated in the magnetic nozzle, where the electric field is removed from the system, allowing a purely diamagnetic situation. The results quantitatively demonstrate the diamagnetism enhanced by the fractional energetic tail electrons for the first time, where the azimuthal internal plasma current can be well described by considering the measured tail electrons in the EEPFs; hence, considering these tail electrons is crucial to understand magnetic field structures modified by plasmas.

Experiments are performed with an electron-beam-excited plasma source connected to a 15 cm diameter and 50 cm long grounded diffusion chamber via a quartz tube as shown in Fig. 1, which has been described previously [21,22]. The beam source consists of a tungsten hot filament and a mesh anode located at  $z = -20$  cm, where  $z = 0$  is the upstream entrance of the diffusion chamber. Argon gas is introduced from the beam source side with a gas flow rate of 5 sccm; the argon pressure measured at the chamber sidewall is about 0.5 mTorr. A pulsed discharge voltage of about 200 V is applied through a  $15 \Omega$  resistor for  $t = 0$ –50 msec between the filament and the anode, creating an electron beam that is injected into the quartz tube. Due to the voltage drop at  $15 \Omega$  resistor, the effective acceleration voltage of the electron beam is about 100 V. Plasma is produced via the electron impact ionization that generates the thermal bulk electrons and cold ions. Two solenoids provide the axial magnetic field, being fairly constant at about 22 mT in the quartz tube and decreasing to about 4 mT at  $z = 20$  cm. As shown by the calculated magnetic field lines in Fig. 1, the field lines expand in the diffusion chamber and form the magnetic nozzle structure. The anode is electrically grounded; the previous experiment has shown that the plasma potential is close to zero [21], resulting in the absence of electric fields [shown later in Fig. 4(f)].

An axially movable B-dot probe (BP) for detecting the axial magnetic field is inserted through a downstream vacuum port. By rotating the (dogleg) probe shaft with a stepping motor, a radial measurement can also be approximately performed. The voltage signal from the BP is proportional to the temporal change in the magnetic flux; the magnetic field induced by the plasma can be obtained by integrating the voltage signal and multiplying by a calibration coefficient. The quas steady-state magnetic field  $\Delta B_z$  induced by the plasma can be estimated from the difference just before and after turning off the plasma.

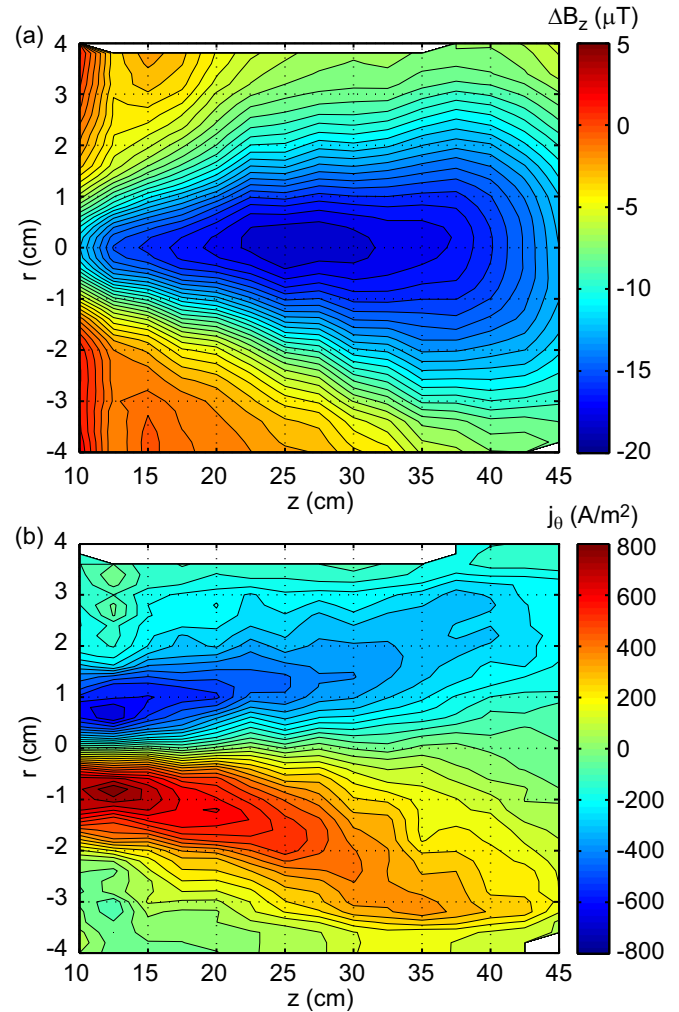


FIG. 2. Two-dimensional profiles of the plasma-induced axial magnetic field  $\Delta B_z$  (a) and the internal azimuthal plasma current density  $j_\theta$  (b), where the measurements are taken at  $\sim 550$  points ( $\sim 37$  and 15 points along  $r$  and  $z$ , respectively).

Two-dimensional mapping of the plasma-induced magnetic field  $\Delta B_z$  in Fig. 2(a) clearly shows a decrease in the axial magnetic field, i.e.,  $\Delta B_z < 0$  characteristic of diamagnetic behavior, over the region of the plasma expansion along the magnetic nozzle. The internal azimuthal current density  $j_\theta$  can be expressed as

$$j_\theta = -\frac{1}{\mu_0} \left( \frac{\partial \Delta B_z}{\partial r} - \frac{\partial \Delta B_r}{\partial z} \right) \sim -\frac{1}{\mu_0} \frac{\partial \Delta B_z}{\partial r} \quad (1)$$

since  $\partial \Delta B_z / \partial r \gg \partial \Delta B_r / \partial z$  has been previously validated [12]. As presented in Fig. 2(b), the azimuthal current density  $j_\theta$  is experimentally determined to be about 600–800 A/m<sup>2</sup> for  $10 < z < 25$  cm and 200–400 A/m<sup>2</sup> for  $25 < z < 45$  cm.

Measurement of the EEPFs is performed by replacing the BP by a cylindrical Langmuir probe (LP). The bias voltage of

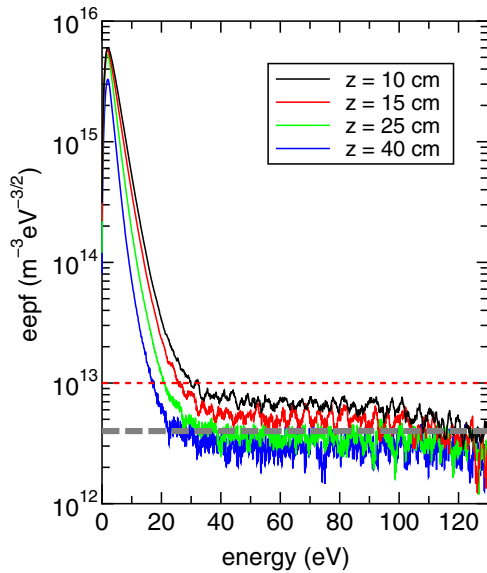


FIG. 3. Typical EPPFs at various  $z$  positions for  $r = 0$ . Data values larger than the noise level (bold horizontal dashed line) and larger than  $10^{13} \text{ m}^{-3} \text{ eV}^{-3/2}$  (horizontal red dotted line) are used to separate the total electron density  $n_e$  and temperature  $T_{\text{eff}}$  from the bulk (only) electron density  $n_{e \text{ bulk}}$  and temperature  $T_{\text{eff bulk}}$ .

the LP is swept from  $-140 \text{ V}$  to  $60 \text{ V}$  for  $t = 20\text{--}50 \text{ msec}$ , where an analog differentiation technique is used to obtain the second derivative. The signals are digitized by a 16-bit data acquisition system and averaged over 50 shots. Strong magnetic field is known to cause some limitation of the EEPF measurement via the second derivative method, but

such measurement is validated for weak magnetic field [23]. In the present study, the electron Larmor radius at  $z \geq 10 \text{ cm}$  is larger than the probe tip radius, and the EEPF measurement is reliable. Figure 3 shows typical EPPFs at various  $z$  positions, showing the thermal bulk electrons with an energy less than about  $20 \text{ eV}$  and the energetic tail electrons with energies up to about  $100 \text{ eV}$  being the remnants of the initial beam with the energy corresponding to the cathode voltage of about  $100 \text{ V}$ . A plausible interpretation for the presence of the tail electrons would be the scattering of the energy and the pitch angle of the source beam electrons by high-frequency plasma waves as has been observed previously [24]. The investigation on such a high frequency instability is out of the scope of the present paper and awaits a further experimental program. It was found that the density of the tail electrons decays and the temperature of the bulk electrons also decreases along the axis. The electron density and effective temperature can be calculated from the EPPFs. The bold horizontal dashed line in Fig. 3 is the maximum noise level in the data acquisition system; signals smaller than the noise level are neglected in the analysis, giving the total density  $n_e$  and temperature  $T_{\text{eff}}$ . Furthermore, the EPPFs of the bulk electrons seem to be fairly Maxwellian and can be analyzed by extracting the data above  $10^{13} \text{ m}^{-3} \text{ eV}^{-3/2}$  (horizontal red dotted line in Fig. 3) in the EPPFs, providing the density  $n_{e \text{ bulk}}$  and temperature  $T_{\text{eff bulk}}$  of the bulk electrons.

Two-dimensional profiles of the bulk and total densities ( $n_{e \text{ bulk}}$ ,  $n_e$ ) and the bulk and total effective temperatures ( $T_{\text{eff bulk}}$ ,  $T_{\text{eff}}$ ) are presented in Figs. 4(a)–4(d), revealing the plasma expansion along the magnetic nozzle. No visible change in the density mappings in Figs. 4(a) and 4(c) can be seen, while the total temperature  $T_{\text{eff}}$  in Fig. 4(d) is much

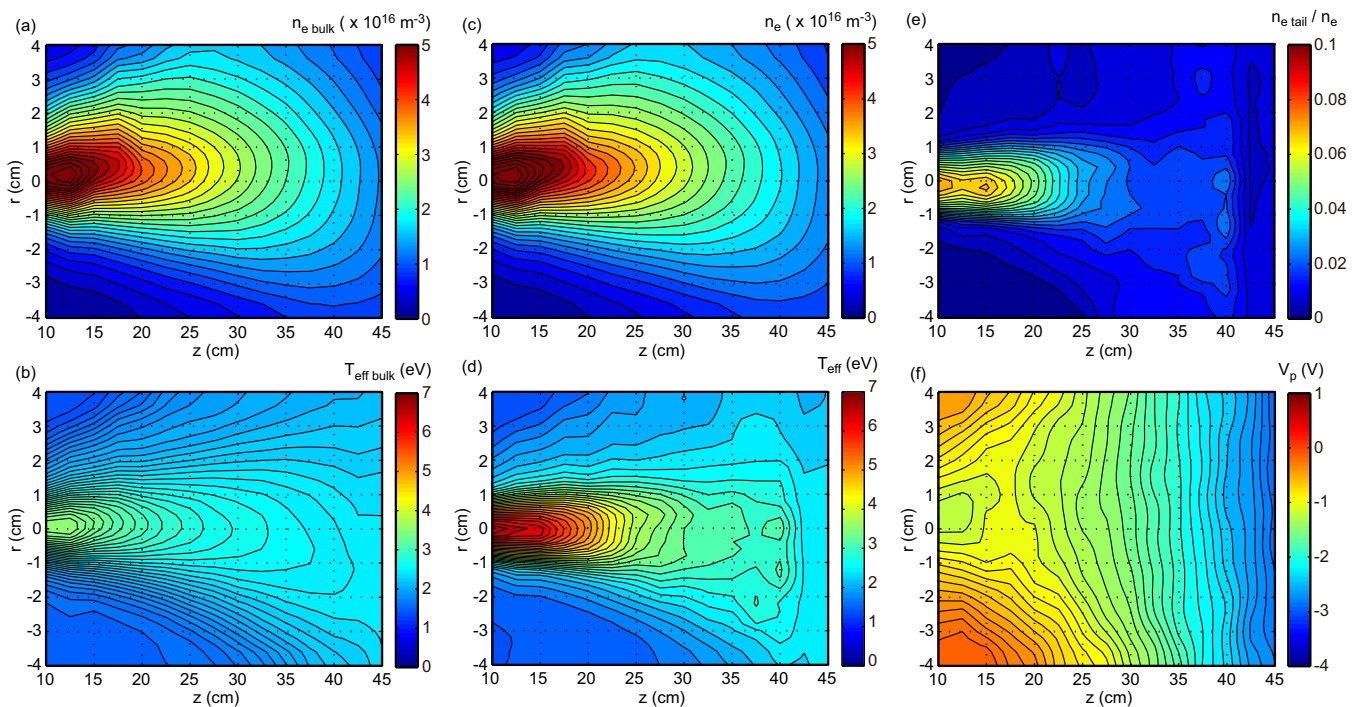


FIG. 4. Two-dimensional profiles of (a) the bulk density  $n_{e \text{ bulk}}$ , (b) the bulk temperature  $T_{\text{eff bulk}}$ , (c) the total density  $n_e$ , (d) the total temperature  $T_{\text{eff}}$ , (e) the density ratio of  $n_{e \text{ tail}}/n_e$ , and (f) the plasma potential  $V_p$  using the same spatial resolution as that of Fig. 2.

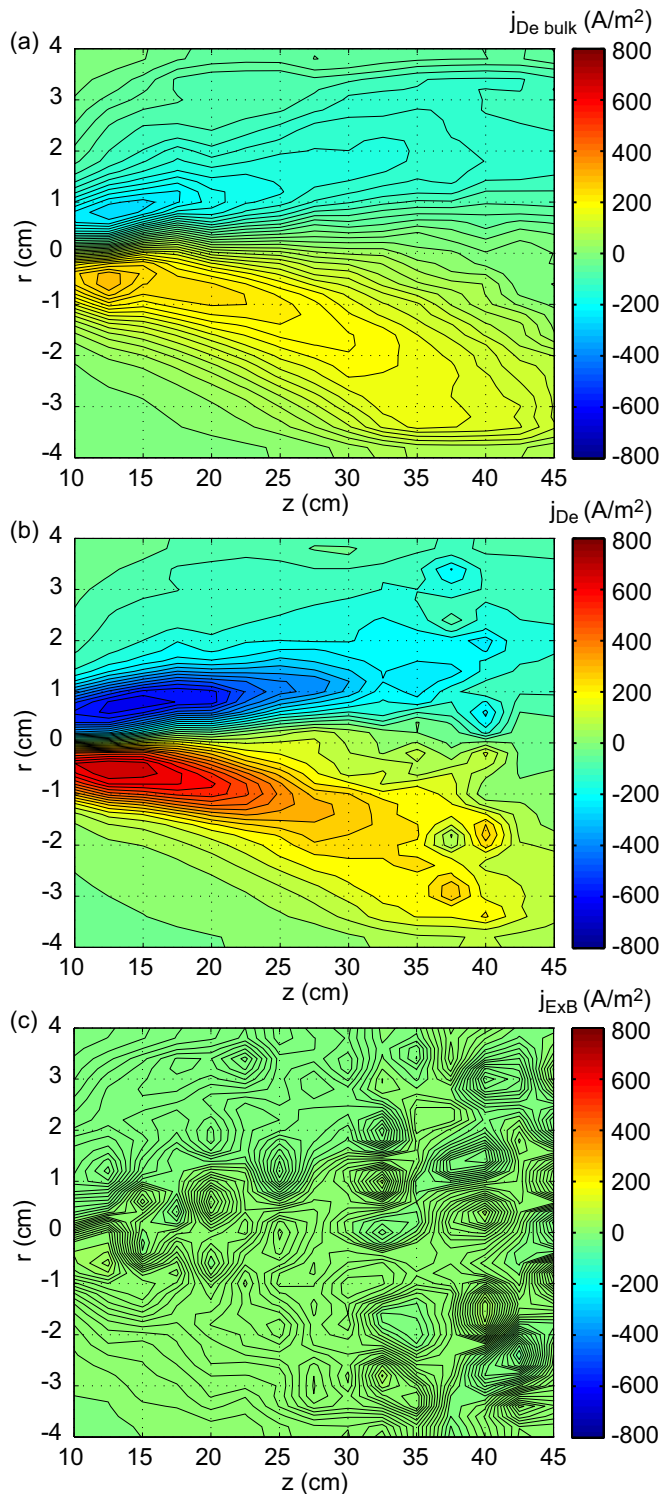


FIG. 5. Two-dimensional profiles of (a) the diamagnetic current density  $j_{De \text{ bulk}}$  by the bulk electrons, (b) the diamagnetic current density  $j_{De}$  by the total electrons, and (c) the  $\mathbf{E} \times \mathbf{B}$  drift current density  $j_{E \times B}$  by the total electrons.

higher than the bulk temperature  $T_{\text{eff bulk}}$  in Fig. 4(b). The density  $n_{e \text{ tail}}$  of the tail electrons can be estimated by  $n_{e \text{ tail}} = n_e - n_{e \text{ bulk}}$  and the ratio of  $n_{e \text{ tail}}/n_e$  is shown in Fig. 4(e), which shows that the tail electron density is less than several percent of the total density. These results imply that a small fraction of energetic tail electrons can significantly increase the effective temperature. Figure 4(f) shows the measured plasma potential  $V_p$  which is very close to zero or slightly lower than zero, validating the neglect of the electric field in the plasma.

As discussed earlier, the plasma diamagnetism is due to internal plasma currents; the electron diamagnetic current due to the bulk and total electrons is calculated from the data in Figs. 4(a)–4(d) as  $(1/B_z)(\partial p_e/\partial r)$  and presented in Figs. 5(a) and 5(b), respectively, where  $p_e$  is the electron pressure. The measured  $(n_{e \text{ bulk}}, T_{\text{eff bulk}})$  and  $(n_e, T_{\text{eff}})$  are used for the calculation of the electron pressures of the bulk and total electrons, respectively. The diamagnetic current density  $j_{De \text{ bulk}}$  generated by the bulk electrons shown in Fig. 5(a) is less than  $200 \text{ A/m}^2$  and is much smaller than the measured current density  $j_\theta$  in Fig. 2(b). However, the diamagnetic current  $j_{De}$ , including both the bulk and tail electrons, can provide the current density of about  $600\text{--}800 \text{ A/m}^2$  for  $10 \text{ cm} < z < 25 \text{ cm}$  as shown in Fig. 5(b), which is very close to the measured  $j_\theta$ . Figure 5(c) shows the electron  $\mathbf{E} \times \mathbf{B}$  drift current density  $j_{E \times B}$  estimated from  $n_e$  in Fig. 4(c) and  $V_p$  in Fig. 4(f), justifying the neglect of the  $\mathbf{E} \times \mathbf{B}$  drift current density. From the results shown above, it is evident that the fractional tail electrons make a major contribution to the diamagnetism of the plasma.

In summary, the diamagnetism, i.e., the plasma-induced magnetic field opposite to the externally applied magnetic field, is investigated under a controlled experiment that is not influenced by the  $\mathbf{E} \times \mathbf{B}$  drift, where the electron energy probability functions include both the low-temperature bulk electrons and the energetic tail electrons. The measurement clearly shows that the azimuthal electric current density is determined by the electron diamagnetic current density including the small fraction of the energetic tail electrons. This result demonstrates that the plasma diamagnetism is enhanced by the non-Maxwellian tail electrons. Since EEPFs containing high energy tail electrons are ubiquitously observed in space, fusion, and laboratory plasmas, the present results require reconsidering non-Maxwellian EEPFs in these broad fields of research when investigating a change in the magnetic field induced by a plasma.

This work was partially supported by the Grant-in-Aid for Scientific Research (Grant No. 19H00663) from the Japan Society for the Promotion of Science and Fusion Oriented Research for disruptive Science and Technology (FOREST) from Japan Science and Technology Agency (Grant No. JP-MJFR212A).

[1] K. D. Cole, Diamagnetism in a plasma, *Phys. Plasmas* **4**, 2072 (1997).

[2] C. T. Russell, The solar wind interaction with the earth's magnetosphere: A tutorial, *IEEE Trans. Plasma Sci.* **28**, 1818 (2000).

- [3] C. Z. Chen, Physics of substorm growth phase, onset, and dipolarization, *Space Sci. Rev.* **113**, 207 (2004).
- [4] F. Plaschke, T. Karlsson, C. Götz, C. Möstl, I. Richter, M. Volwerk, A. Eriksson, E. Behar, and R. Goldstein, First observations of magnetic holes deep within the coma of a comet, *Astron. Astrophys.* **618**, A114 (2018).
- [5] M. Tuszewski, Field reversed configurations, *Nucl. Fusion* **28**, 2033 (1988).
- [6] A. Fruchtman, Electric Field in a Double Layer and the Imparted Momentum, *Phys. Rev. Lett.* **96**, 065002 (2006).
- [7] E. Ahedo and M. Merino, Two-dimensional supersonic plasma acceleration in a magnetic nozzle, *Phys. Plasmas* **17**, 073501 (2010).
- [8] K. Takahashi, C. Charles, and R. W. Boswell, Approaching the Theoretical Limit of Diamagnetic-Induced Momentum in a Rapidly Diverging Magnetic Nozzle, *Phys. Rev. Lett.* **110**, 195003 (2013).
- [9] R. L. Stenzel and J. M. Urrutia, Electron magnetohydrodynamic turbulence in a high-beta plasma. I. plasma parameters and instability conditions, *Phys. Plasmas* **7**, 4450 (2000).
- [10] C. S. Corr and R. W. Boswell, High-beta plasma effects in a low-pressure helicon plasma, *Phys. Plasmas* **14**, 122503 (2007).
- [11] A. Fruchtman and S. Shinohara, Diamagnetism and neutrals depletion in a plasma, *Phys. Plasmas* **24**, 103523 (2017).
- [12] K. Takahashi, A. Chiba, A. Komuro, and A. Ando, Experimental identification of an azimuthal current in a magnetic nozzle of a radiofrequency plasma thruster, *Plasma Sources Sci. Technol.* **25**, 055011 (2016).
- [13] H. Zhao, B. Ni, X. Li, D. N. Baker, W. R. Johnston, W. Zhang, Z. Xiang, X. Gu, A. N. Jaynes, S. G. Kanekal, J. B. Blake, S. G. Claudepierre, M. A. Temerin, H. O. Funsten, G. D. Reeves, and A. J. Boyd, Plasmaspheric hiss waves generate a reversed energy spectrum of radiation belt electrons, *Nat. Phys.* **15**, 367 (2019).
- [14] H. Che and M. L. Goldstein, The origin of non-Maxwellian solar wind electron velocity distribution function: Connection to nanoflares in the solar corona, *Astrophys. J., Lett.* **795**, L38 (2014).
- [15] A. L. Milder, J. Katz, R. Boni, J. P. Palastro, M. Sherlock, W. Rozmus, and D. H. Froula, Measurements of Non-Maxwellian Electron Distribution Functions and Their Effect on Laser Heating, *Phys. Rev. Lett.* **127**, 015001 (2021).
- [16] A. E. Shevelev, E. M. Khilkevitch, V. G. Kiptily, I. N. Chugunov, D. B. Gin, D. N. Doinikov, V. O. Naidenov, A. E. Litvinov, I. A. Polunovskii, and JET-EFDA Contributors, Reconstruction of distribution functions of fast ions and runaway electrons in fusion plasmas using gamma-ray spectrometry with applications to ITER, *Nucl. Fusion* **53**, 123004 (2013).
- [17] S.-H. Seo, J.-H. In, and H.-Y. Chang, Measurements of electron energy distribution functions and electron transport in the downstream region of an unbalanced dc magnetron discharge, *Plasma Sources Sci. Technol.* **13**, 409 (2004).
- [18] C. W. Chung, S. S. Kim, and H. Y. Chang, Electron Cyclotron Resonance in a Weakly Magnetized Radio-Frequency Inductive Discharge, *Phys. Rev. Lett.* **88**, 095002 (2002).
- [19] D. Hemmers, H. Kempkens, and J. Uhlenbusch, Investigation of the electron energy distribution in an ECR discharge by means of Thomson scattering, *J. Phys. D: Appl. Phys.* **34**, 2315 (2001).
- [20] C. Charles, High density conics in a magnetically expanding helicon plasma, *Appl. Phys. Lett.* **96**, 051502 (2010).
- [21] K. Takahashi, C. Charles, R. Boswell, and A. Ando, Adiabatic Expansion of Electron Gas in a Magnetic Nozzle, *Phys. Rev. Lett.* **120**, 045001 (2018).
- [22] K. Takahashi, C. Charles, R. W. Boswell, and A. Ando, Thermodynamic Analogy for Electrons Interacting with a Magnetic Nozzle, *Phys. Rev. Lett.* **125**, 165001 (2020).
- [23] T. K. Popov, M. Dimitrova, P. Ivanova, J. Kovačič, T. Gyergyek, R. Dejarnac, J. Stöckel, M. A. Pedrosa, D. López-Bruna, and C. Hidalgo, Advances in Langmuir probe diagnostics of the plasma potential and electron-energy distribution function in magnetized plasma, *Plasma Sources Sci. Technol.* **25**, 033001 (2016).
- [24] R. W. Boswell, S. M. Hamberger, P. J. Kellogg, I. Morey, and R. K. Porteous, Direct observation of rapid impulsive electron heating during a beam plasma interaction, *Phys. Lett. A* **101**, 501 (1984).